

AFLOW-QHA3P: Robust and automated method to compute thermodynamic properties of solids

Pinku Nath,^{1,2} Demet Usanmaz,^{1,2} David Hicks,^{1,2} Corey Oses,^{1,2} Marco Fornari,^{3,2}
Marco Buongiorno Nardelli,^{4,2} Cormac Toher,^{1,2} and Stefano Curtarolo^{1,2,5,*}

¹*Department of Mechanical Engineering and Materials Science, Duke University, Durham, North Carolina 27708, USA*

²*Center for Materials Genomics, Duke University, Durham, NC 27708, USA*

³*Department of Physics, Central Michigan University, Mount Pleasant, MI 48858, USA*

⁴*Department of Physics and Department of Chemistry, University of North Texas, Denton TX, USA*

⁵*Fritz-Haber-Institut der Max-Planck-Gesellschaft, 14195 Berlin-Dahlem, Germany*

(Dated: June 29, 2021)

Accelerating the calculations of finite-temperature thermodynamic properties is a major challenge for rational materials design. Reliable methods can be quite expensive, limiting their effective applicability in autonomous high-throughput workflows. Here, the 3-phonons quasi-harmonic approximation (QHA) method is introduced, requiring only three phonon calculations to obtain a thorough characterization of the material. Leveraging a Taylor expansion of the phonon frequencies around the equilibrium volume, the method efficiently resolves the volumetric thermal expansion coefficient, specific heat at constant pressure, the enthalpy, and bulk modulus. Results from the standard QHA and experiments corroborate the procedure, and additional comparisons are made with the recently developed self-consistent QHA. The three approaches — 3-phonons, standard, and self-consistent QHAs — are all included within the automated, open-source framework AFLOW, allowing automated determination of properties with various implementations within the same framework.

INTRODUCTION

Reliable and efficient computational methods are needed to guide time-consuming and laborious experimental searches, thus accelerating materials design. Implementing effective methods within automated frameworks such as AFLOW [1–5] facilitates the calculation of thermodynamic properties for large materials databases. There are several computational techniques to characterize the temperature dependent properties of materials, each with varying accuracy and computational cost. Techniques such as *ab initio* molecular dynamics [6–10] and the stochastic self-consistent harmonic approximation [11, 12] give accurate results for the temperature dependent properties of materials. Although these methods are highly accurate, the treatment of anharmonicity requires the consideration of many large distorted structural configurations, making them computationally prohibitive for screening large materials sets. Other methods including the Debye-Grüneisen model [13, 14] or Machine Learning approaches [15, 16] require less computational resources, but often struggle to predict properties such as the Grüneisen parameter with reasonable accuracy [17, 18]. The quasi-harmonic approximation (QHA) [19–21] balances accuracy and computational cost for calculating temperature and pressure dependent properties of materials.

In its standard formulation, QHA also remains too expensive for automated screening [22]. QHA requires many independent phonon spectra calculations, obtained by diagonalizing the dynamical matrices giving eigenvectors (modes) and eigenvalues (energies) [23–26]. The dynamical matrix can be constructed either with “linear re-

sponse” [26, 27] or the “finite displacements” method [26, 28, 29]. Despite its low computational demands, linear response does not perform well at high temperatures where anharmonicity can be large. The finite displacements method can be easily integrated with a routine that computes forces, making the preferred method for high-throughput calculations. However, it is still computationally expensive for (i) low symmetry crystals, (ii) materials with large atomic variations leading to complicated optical branches, and (iii) metallic systems having long-range force interactions requiring large supercells. In order to make QHA more suitable for automated screening, it is necessary to reduce the number of required phonon spectra.

Recently, the self-consistent quasi-harmonic approximation [30] (SC-QHA) has been developed. It self-consistently minimizes the external and internal pressures. The method requires spectra at only two or three volumes, while the frequency-volume relationship is determined using a Taylor expansion. It is computationally efficient and almost five times faster than QHA. Results agree well with experiments at low temperatures, although some deviations are observed at high-temperature for the tested systems [30].

In this article, the quasi-harmonic approximation 3-phonons (QHA3P) method is introduced. It calculates the phonon frequencies around equilibrium for only three different volumes, and performs a Taylor expansion to extrapolate the phonon frequencies at other volumes. The QHA3P approach drastically reduces the computational cost and achieves consistency with experiments, allowing automated materials’ property screening without compromising accuracy. Similar to QHA, QHA3P minimizes the Helmholtz free energy with respect to volume for each temperature. The calculation of the thermodynamic properties, and the temperature dependent electronic contribution to the free energy, are the same as in QHA, enabling

* stefano@duke.edu

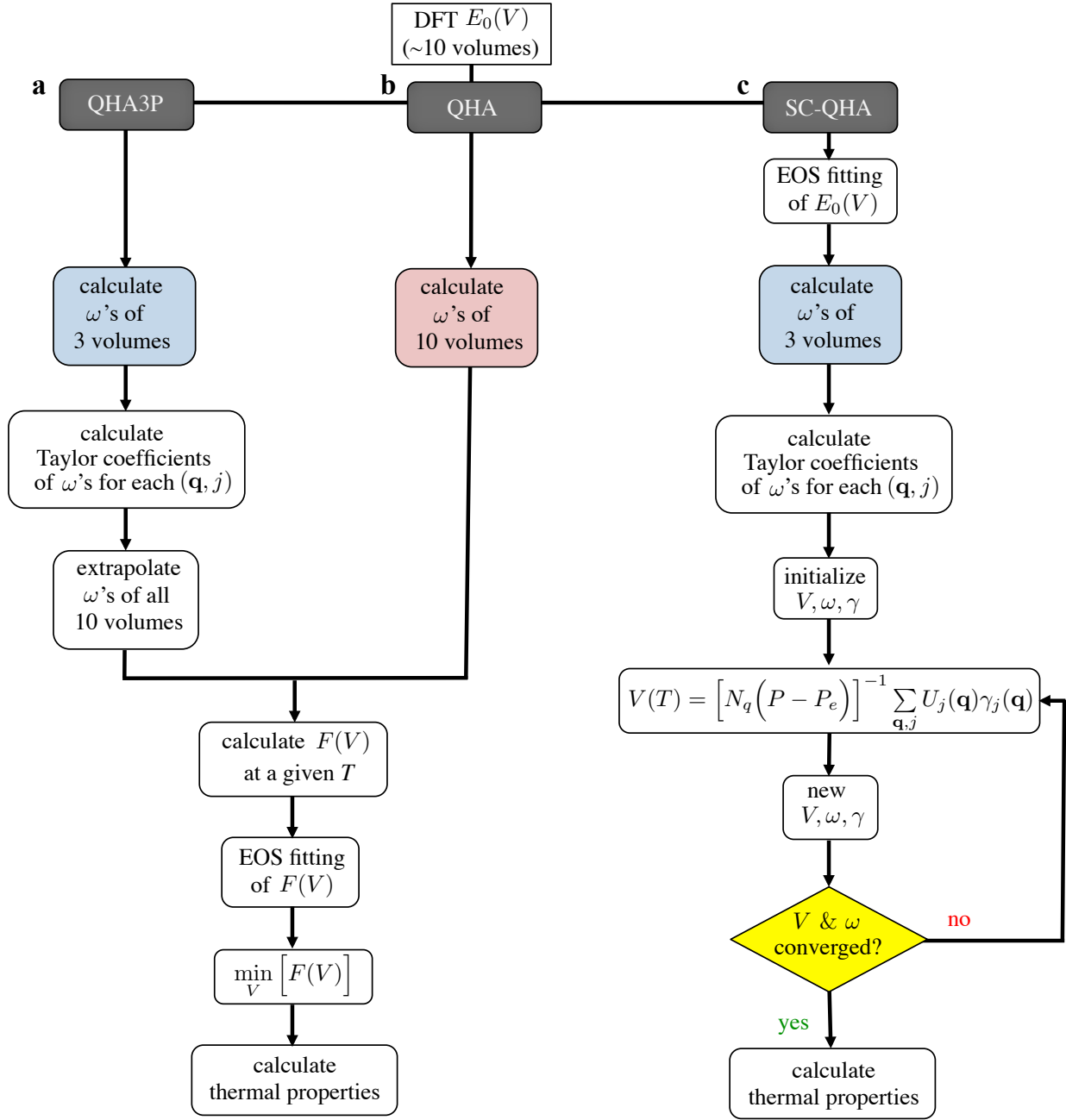


Figure 1. The workflows for (a) QHA3P compared with (b) QHA and (c) SC-QHA. The most time-consuming step of QHA is highlighted in red, while the time-saving steps of the other two methods are highlighted in blue.

unrestricted screening of all types of materials. The QHA, SC-QHA, and QHA3P methods are all implemented within AFLOW [1–5, 22]. The performance of QHA3P with two different `exchange-correlation` (XC) functionals is investigated.

COMPUTATIONAL DETAILS

The thermal properties of materials at finite temperatures are calculated from the Helmholtz free energy (F), which depends on temperature (T) and volume (V). Ne-

glecting the electron-phonon coupling and magnetic contributions, F can be written as the sum of three additive contributions [19–21]:

$$F(V, T) = E_0(V) + F_{\text{vib}}(V, T) + F_{\text{elec}}(V, T), \quad (1)$$

where E_0 is the total energy of the system at 0 K without any atomic vibrations, F_{vib} is the vibrational free energy of the lattice ions, and F_{elec} is the finite temperature electronic free energy due to thermal electronic excitations.

QHA Methodology. QHA enables the calculation of F_{vib}

via the harmonic approximation and includes anharmonic

effects in the form of volume dependent phonon frequencies. F_{vib} is given by [19–22]:

$$F_{\text{vib}}(V, T) = \frac{1}{N_q} \sum_{\mathbf{q}, j} \left(\frac{\hbar \omega_j(\mathbf{q})}{2} + k_B T \ln \left[1 - \exp \left(-\frac{\hbar \omega_j(\mathbf{q})}{k_B T} \right) \right] \right), \quad (2)$$

where \hbar and k_B are the Planck and Boltzmann constants, and $\omega_j(\mathbf{q})$ is the volume dependent phonon frequency (at \mathbf{q}, j). The (\mathbf{q}, j) comprises both the wave vector \mathbf{q} and phonon branch index j . N_q is the total number of wave vectors.

Although $F_{\text{elec}}(V, T)$ is negligible for wide band gap materials, its contribution is required for metals and narrow band-gap systems. $F_{\text{elec}}(V, T)$ is calculated as [19, 20, 31]:

$$\begin{aligned} F_{\text{elec}}(V, T) &= U_{\text{elec}}(V, T) - T S_{\text{elec}}(V, T), \\ U_{\text{elec}}(V, T) &= \int_0^{\infty} n_{\text{elec}}(\epsilon) f(\epsilon) \epsilon d\epsilon - \int_0^{E_F} n_{\text{elec}}(\epsilon) \epsilon d\epsilon, \\ S_{\text{elec}}(V, T) &= -k_B \int_0^{\infty} n_{\text{elec}}(\epsilon) [f(\epsilon) \ln(f(\epsilon)) + \\ &\quad + (1 - f(\epsilon)) \ln(1 - f(\epsilon))] d\epsilon, \end{aligned} \quad (3)$$

where $U_{\text{elec}}(V, T)$ and $S_{\text{elec}}(V, T)$ are the temperature dependent parts of the electronic internal energy and the electronic entropy respectively, $n_{\text{elec}}(\epsilon)$ is the density of states at energy ϵ , $f(\epsilon)$ is the Fermi-Dirac distribution, and E_F is the Fermi energy.

The QHA method requires at least $\sim 10 E_0$ and ~ 10 phonon calculations (F_{vib}) in order to obtain a good fit for the equation of state (EOS). QHA is generally implemented using isotropic volume distortions, although its implementation in AFLOW can also include anisotropic effects by considering F as a function of direction-dependent strain, *e.g.* along principal directions [32, 33]. The calculated E_0 and F_{vib} are fitted to an EOS (*e.g.*, Birch-Murnaghan EOS [34]). The equilibrium volume (V_{eq}) at a given temperature is determined by minimizing F with respect to V at a given T , $(\partial F / \partial V)_T = 0$ (Figure 1b). A more detailed description of F - V interpolation and the calculation of different energy terms is discussed in Ref. [22].

The thermodynamic properties — constant volume specific heat (C_V), constant pressure specific heat (C_P), average Grüneisen parameter ($\bar{\gamma}$), and volumetric thermal expansion coefficient (α_V) [19–22] — are calculated according to the following definitions:

$$C_V = k_B \sum_{\mathbf{q}, j} \left(\frac{\hbar \omega_j(\mathbf{q}, V_0)}{k_B T} \right)^2 \frac{\exp \left(\frac{\hbar \omega_j(\mathbf{q}, V_0)}{k_B T} \right)}{\left(\exp \left(\frac{\hbar \omega_j(\mathbf{q}, V_0)}{k_B T} \right) - 1 \right)^2} \quad (4)$$

$$C_P = C_V + V_{\text{eq}} T B \alpha_V^2, \quad (5)$$

$$\bar{\gamma} = \frac{\sum_{\mathbf{q}, j} \gamma_j(\mathbf{q}) c_j(\mathbf{q})}{\sum_{\mathbf{q}, j} c_j(\mathbf{q})}, \quad (6)$$

$$\alpha_V = \frac{C_V \bar{\gamma}}{B V_{\text{eq}}}, \quad (7)$$

where $\omega_j(\mathbf{q}, V_0)$ is the frequency of phonon mode (\mathbf{q}, j) at relaxed volume (V_0), and $c_j(\mathbf{q})$ and $\gamma_j(\mathbf{q})$ are the specific heat capacity at constant volume and mode Grüneisen at (\mathbf{q}, j) . The definitions of the bulk modulus (B) and mode Grüneisen parameter, ($\gamma_j(\mathbf{q})$), are

$$B = V_{\text{eq}} \left(\frac{\partial^2 F}{\partial V^2} \right)_T, \quad (8)$$

$$\gamma_j(\mathbf{q}) = -\frac{V_0}{\omega_j(\mathbf{q}, V_0)} \left(\frac{\partial \omega_j(\mathbf{q})}{\partial V} \right)_{V_0}, \quad (9)$$

For metals and small band gap materials, the electronic contribution can be considerable and is included in the thermodynamic definitions. After including the electronic contribution, α_V and C_P are re-formulated as [33, 35]:

$$\begin{aligned} \alpha_{V, \text{ph+elec}} &= \alpha_V + \alpha_{V, \text{elec}} = \frac{C_V \bar{\gamma}}{B V_{\text{eq}}} + \frac{2}{3 B V_{\text{eq}}} C_{V, \text{elec}}, \\ C_{P, \text{ph+elec}} &= C_V + V_{\text{eq}} T B \alpha_V^2 + C_{V, \text{elec}}, \end{aligned} \quad (10)$$

$$C_{V, \text{elec}} = T \left(\frac{\partial S_{\text{elec}}}{\partial T} \right)_V.$$

In addition to the basic quasi-harmonic thermodynamic properties, the enthalpy (H) of a structure at $P=0$ [21, 31] is:

$$H = F(T) + T S = F(T) - T \frac{\partial F(T)}{\partial T}. \quad (11)$$

AFLOW implementation of SC-QHA. SC-QHA has also been implemented within AFLOW following the description of Ref. [30]. Similar to QHA, SC-QHA calculates E_0 at ~ 10 different volumes, but requires only

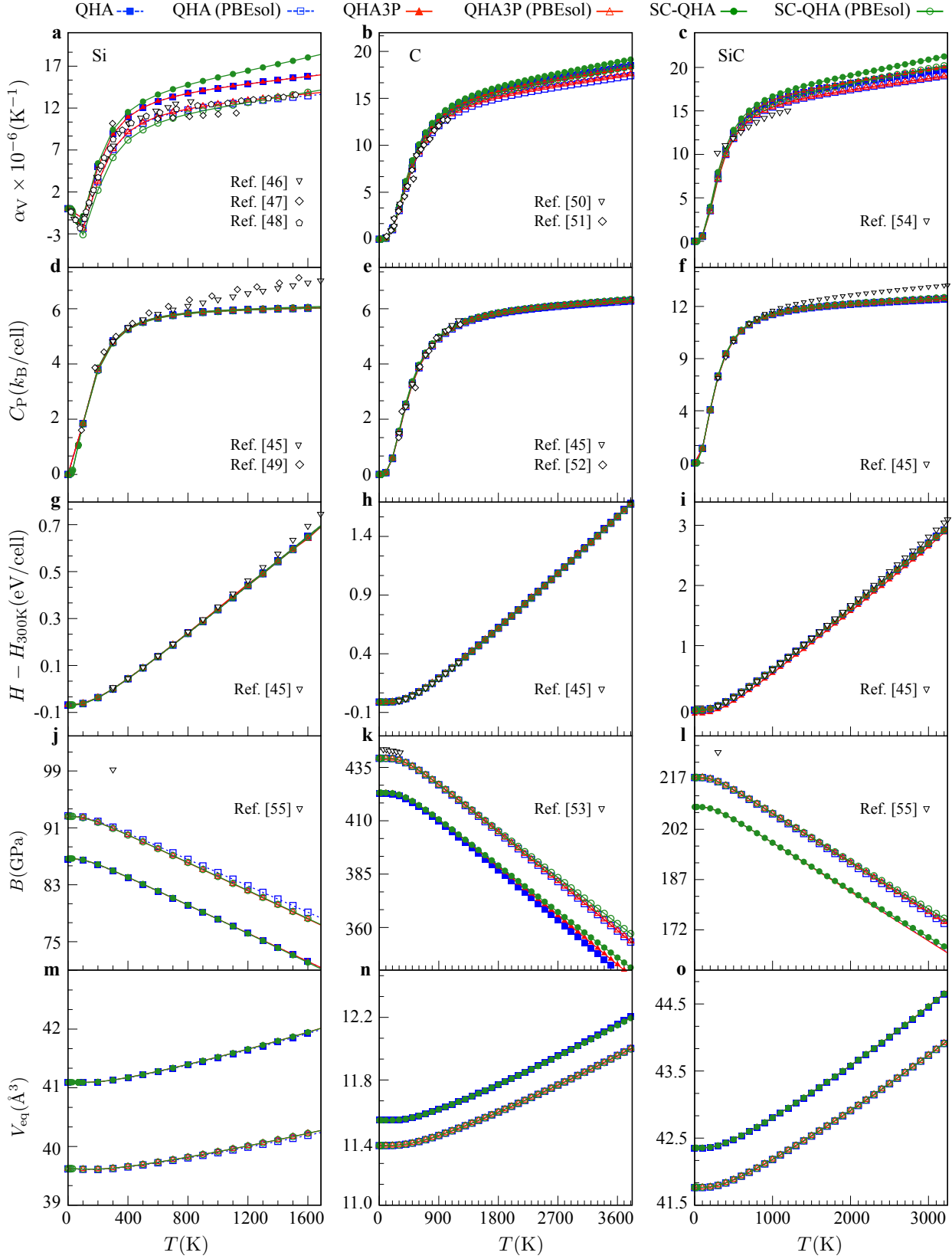


Figure 2. The thermodynamic properties of Si (a,d,g,j,m), C (b,e,h,k,n), and SiC (c,f,i,l,o) are presented up to their melting temperatures (T_m): 1687, 3823 and 3000 K [36], respectively. The results are obtained with QHA3P, QHA and SC-QHA using the PBE and PBEsol XC functionals. Experimental results from different sources [36–46] are indicated by inverted triangles, diamonds, and pentagons.

three phonon calculations at different cell volumes (Figure 1c) [30]. It computes the temperature-dependent unit-cell volume by optimizing the total pressure (external, electronic, and phononic pressures),

$$V = [(P - P_e)]^{-1} \times \frac{1}{N_q} \sum_{\mathbf{q}, j} U_j(\mathbf{q}) \gamma_j(\mathbf{q}), \quad (12)$$

where P is external pressure, $P_e (= -dE_0(V)/dV)$ is the electronic pressure, $U_j(\mathbf{q})$ is the mode vibrational internal energy and $\gamma_j(\mathbf{q})$ is the mode Grüneisen parameter at (\mathbf{q}, j) . The volume dependent $\omega_j(\mathbf{q})$ and $\gamma_j(\mathbf{q})$ are extrapolated to other volumes using a Taylor expansion:

$$\begin{aligned} \omega_j(\mathbf{q}, V) &= \omega_j(\mathbf{q}, V_0) + \left(\frac{\partial \omega_j(\mathbf{q})}{\partial V} \right)_{V_0} (\Delta V) \\ &+ \frac{1}{2} \left(\frac{\partial^2 \omega_j(\mathbf{q})}{\partial V^2} \right)_{V_0} (\Delta V)^2, \end{aligned} \quad (13)$$

$$\gamma_j(\mathbf{q}, V) = -\frac{V}{\omega_j(\mathbf{q})} \left[\left(\frac{\partial \omega_j(\mathbf{q})}{\partial V} \right)_{V_0} + \left(\frac{\partial^2 \omega_j(\mathbf{q})}{\partial V^2} \right)_{V_0} \Delta V \right], \quad (14)$$

where $\Delta V = V - V_0$. Computing the second order derivative of $\omega_j(\mathbf{q})$ requires the calculation of phonon spectra at three different volumes. Due to its numerical accuracy, the central difference algorithm is used to calculate the derivative with respect to volume. $U_j(\mathbf{q})$, the mode vibrational internal energy, is defined as

$$U_j(\mathbf{q}) = \left[\left(\exp \left(\frac{\hbar \omega_j(\mathbf{q})}{k_B T} \right) - 1 \right)^{-1} + \frac{1}{2} \right] \hbar \omega_j(\mathbf{q}). \quad (15)$$

The procedure to self-consistently optimize the volume at zero external pressure ($P=0$) and finite T is as follows [30] (Figure 1c):

- (1) First, $\sim 10 E_0(V)$ values are fitted to the EOS, enabling the analytical calculation of P_e at any new volume.
- (2) $(\partial \omega_j(\mathbf{q})/\partial V)_{V_0}$ and $(\partial^2 \omega_j(\mathbf{q})/\partial V^2)_{V_0}$ are calculated from the three phonon spectra, where $\omega_j(\mathbf{q})$ and $\gamma_j(\mathbf{q})$ are initialized to their values at V_0 .
- (3) To compute the equilibrium volume at T , V is initialized to a value 0.2% larger than V_0 and the following loop is iterated:
 - (i) Calculate P_e using the EOS, and $\sum_{\mathbf{q}, j} U_j(\mathbf{q}) \gamma_j(\mathbf{q})$ using $\omega_j(\mathbf{q})$ and $\gamma_j(\mathbf{q})$.
 - (ii) Update the value of V using Eq. (12), and update $\omega_j(\mathbf{q})$ and $\gamma_j(\mathbf{q})$ using Eq. (13 - 14), respectively.
 - (iii) If V is not converged to within an acceptable threshold (e.g., 10^{-6}), then loop over steps (i) and (ii).

- (iv) Calculate other thermodynamic properties using the converged values of $\omega_j(\mathbf{q})$ and $\gamma_j(\mathbf{q})$.
- (v) V , $\omega_j(\mathbf{q})$, and $\gamma_j(\mathbf{q})$ values at a given T are used as the initial values for the next T characterization.

In SC-QHA, at low temperatures (e.g., 0.1 K), V_{eq} is calculated self-consistently. At higher temperatures, V_{eq} is extrapolated as $V_{\text{eq}}(T + \Delta T) \simeq (1 + \alpha_V \Delta T) V_{\text{eq}}$, as described in Ref. [30], in order to avoid self-consistent volume calculations for each T . V_{eq} is equal to the self-consistently converged V at a given T . Similarly, all of the properties calculated at V_{eq} are the equilibrium properties at T .

While C_V , C_P , and α_V are the same as for QHA, B and $\gamma_j(\mathbf{q})$ are computed differently in SC-QHA. Here:

$$B = V_{\text{eq}} \left(\frac{d^2 E_0}{dV^2} \right)_{V_{\text{eq}}} + B_\gamma + B_{\Delta\gamma} + P_\gamma, \quad (16)$$

where B_γ and $B_{\Delta\gamma}$ are the bulk modulus contributions due to phonons, while P_γ represents the bulk modulus contribution due to external pressure. The mathematical expressions for these variables are defined in Ref. [30], and $\gamma_j(\mathbf{q})$ is computed using Eq. (14). It is also important to note that the value of C_V at given T is computed with the $\omega_j(\mathbf{q})$ values instead of $\omega_j(\mathbf{q}, V_0)$, where $\omega_j(\mathbf{q})$ is the volume (and thus temperature) dependent frequency.

The temperature dependent electronic energy contributions can be added to SC-QHA by establishing the relationship between the electronic eigenvalues and V (similar to the relationship between phonon eigenvalues and volume (Eq. 12)). F_{elec} is not included in the version of SC-QHA implemented in AFLOW. Derivations and a more detailed description of SC-QHA can be found in Ref. [30]. The version of SC-QHA implemented in AFLOW is equivalent to the 2nd-SC-QHA.

QHA3P Methodology. The QHA3P method requires only three phonon calculations along with the $\sim 10 E_0$ energies. The Taylor expansion (Eq. 13) introduced in SC-QHA [30], is used to extrapolate the phonon spectra to the remaining volumes. The following steps are the same as QHA: fit to the EOS, minimize F with respect to V , and calculate the thermodynamic properties (Figure 1a).

Although the same technique is used to extrapolate the phonon frequencies (Eq. 13)) in both QHA3P and SC-QHA, the definitions of some thermodynamic properties and the method of computing them are different. For example, the mode Grüneisen in QHA3P is calculated using Eq. (9), whereas in SC-QHA it is obtained using Eq. (14). In SC-QHA, $\gamma_j(\mathbf{q})$ is temperature dependent, whereas it is temperature independent in QHA3P and QHA.

Implications of T dependent $\gamma_j(\mathbf{q})$ in SC-QHA. The main contribution to Eq. (14) comes from V_{eq} , $\omega_j(\mathbf{q})$, and $(\partial \omega_j(\mathbf{q})/\partial V)_{V_0}$. The second term is neglected due to the small size of $(\partial^2 \omega_j(\mathbf{q})/\partial V^2)_{V_0}$.

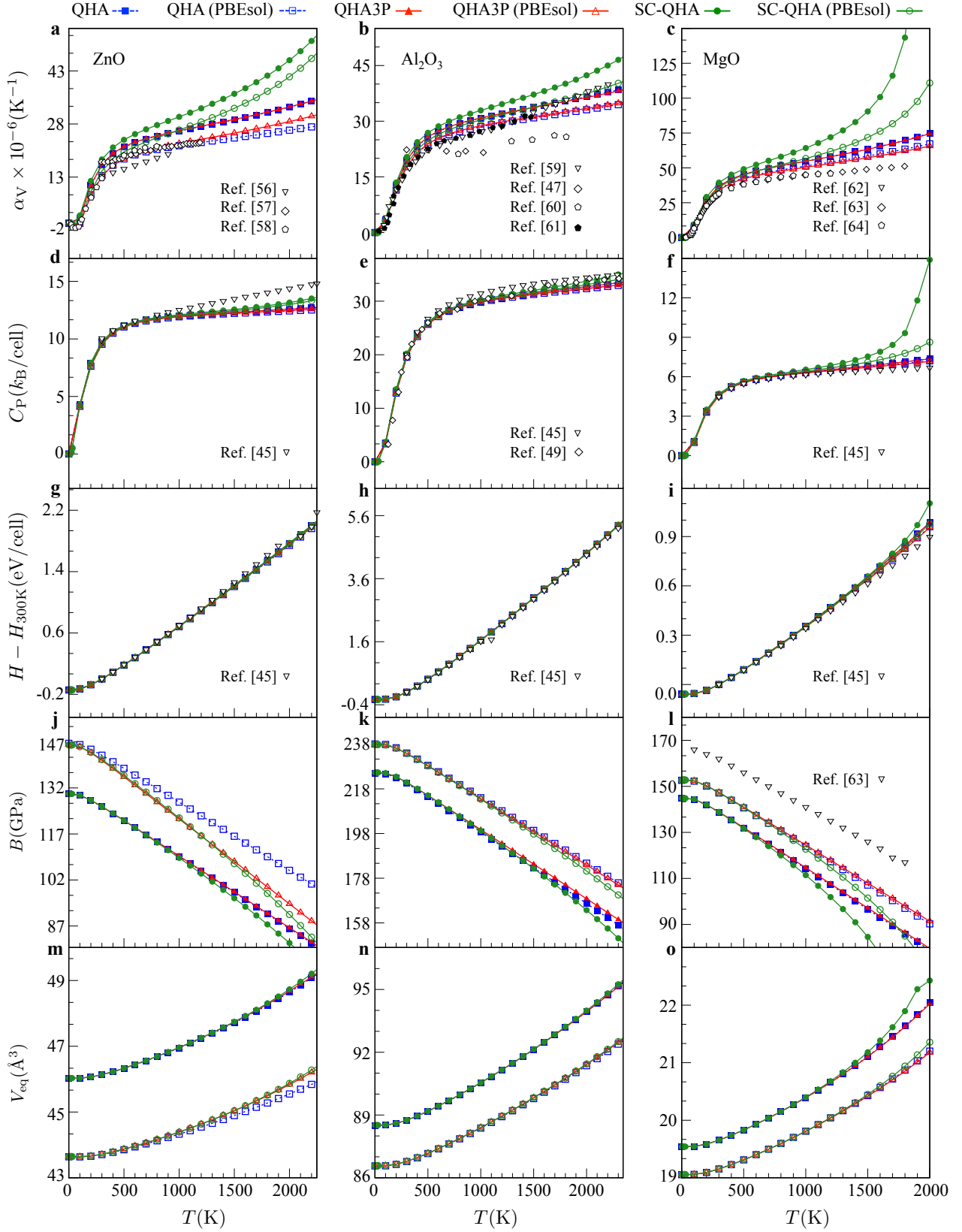


Figure 3. The thermodynamic properties of ZnO (a,d,g,j,m), Al₂O₃ (b,e,h,k,n), and MgO (c,f,i,l,o) as a function of temperature. The results of ZnO and Al₂O₃ are presented up to T_m , while MgO is shown up to $(2/3)T_m$. The T_m values of ZnO, Al₂O₃ and MgO are 2248, 2345 and 3125 K [36], respectively. The results are obtained with QHA3P, QHA and SC-QHA using the PBE and PBEsol XC functionals. Experimental results from different sources [36, 38, 47–55] are indicated by inverted triangles, diamonds, pentagons, and filled pentagons.

- In SC-QHA, $\gamma_j(\mathbf{q})$ is temperature dependent due to the prefactor $V_{\text{eq}}(T)/\omega_j(\mathbf{q}, V_{\text{eq}}(T))$ (Eq. (14)).
- If V_{eq} changes positively with T and $(\partial\omega_j(\mathbf{q})/\partial V)_{V_0} < 0$, then $\gamma_j(\mathbf{q})$ increases with T (Eq. (14)).
- $\omega_j(\mathbf{q}, V_{\text{eq}}(T))$ should decrease with increasing T if the above condition is valid (Eq. (13)), amplifying the T dependence of $\gamma_j(\mathbf{q})$.
- If $\gamma_j(\mathbf{q})$ increases for the majority of (\mathbf{q}, j) in the Brillouin zone, then $\bar{\gamma}$ will be overestimated by SC-QHA in comparison to QHA3P and QHA.
- $(\partial\omega_j(\mathbf{q})/\partial V)_{V_0}$ is negative when $\omega_j(\mathbf{q})$ decreases with T . The behavior of $(\partial\omega_j(\mathbf{q})/\partial V)_{V_0}$ is described by the following expressions [56]:

$$\begin{aligned} \left. \frac{d\omega_j(\mathbf{q})}{dT} \right|_{\text{P}} &= \left(\frac{\partial\omega_j(\mathbf{q})}{\partial V} \right)_{\text{P}} \left. \frac{\partial V}{\partial T} \right|_{\text{P}} \\ \Rightarrow \left(\frac{\partial\omega_j(\mathbf{q})}{\partial V} \right)_{\text{P}} &= \frac{1}{V\alpha_V} \left. \frac{d\omega_j(\mathbf{q})}{dT} \right|_{\text{P}}. \end{aligned} \quad (17)$$

Thus, SC-QHA always produces larger $\bar{\gamma}$ values than QHA3P and QHA for materials where $\omega_j(\mathbf{q})$ decreases with T for the majority of (\mathbf{q}, j) , and that have positive thermal expansion. This applies to positive thermal expansion materials (all of the materials in this study). The effect of this on α_V is discussed in the next section.

The root-mean-square relative deviation. The root-mean-square relative deviation (RMSrD)

$$\chi(X, Y) = \sqrt{\frac{\sum_i^N \left(\frac{X_i - Y_i}{X_i} \right)^2}{N - 1}} \quad (18)$$

is used to quantitatively compare the calculated thermodynamic properties between the various methods, and to validate the model against experiments. Here $\chi(X, Y)$ represents the RMSrD between N data points obtained from methods X and Y . Small values of $\chi(X, Y)$ indicate that X and Y produce statistically similar results.

Geometry optimization. All structures are fully relaxed using the high-throughput framework AFLOW, and density functional theory package VASP [57]. Optimizations are performed following the AFLOW standard [58]. The projector augmented wave (PAW) pseudopotentials [59] and the XC functionals proposed by Perdew-Burke-Ernzerhof (PBE) [60] are used for all calculations, unless otherwise stated. To study functional effects and compare with previous SC-QHA results [30], calculations using the PBEsol functional [61] are also carried out. A high energy cutoff (40% larger than the maximum recommended cutoff among all the species) and a

TABLE I. Compound names with ICSD number, supercell size, supercell atoms, lattice type, and sg #. More detailed information is available in Table A1 Appendix.

compound	ICSD	supercell size	supercell atoms	lattice type	sg #
Si	76268	5×5×5	250	fcc	227
C (Diamond)	28857	4×4×4	128	fcc	227
SiC	618777	4×4×3	192	hex	186
Al ₂ O ₃	89664	2×2×2	80	rhl	167
MgO	159372	4×4×4	128	fcc	225
ZnO	182356	4×4×3	192	hex	186
AlNi	602150	4×4×4	128	cub	221
NiTiSn	174568	3×3×3	81	fcc	216
Ti ₂ AlN	157766	4×4×1	128	hex	194

k-point mesh of 8000 **k**-points per reciprocal atom are used to ensure the accuracy of the results. Primitive cells are fully relaxed until the energy difference between two consecutive ionic steps is smaller than 10^{-9} eV and forces on each atom are below 10^{-8} eV/Å.

Phonon calculations. Phonon calculations are carried out using the Automatic Phonon Library [29, 62], as implemented in AFLOW, using VASP to obtain the interatomic force constants via the finite-displacements approach. The magnitude of this displacement is chosen as 0.015Å. Supercell size and the number of atoms in the supercell (supercell atoms) along with space group number (sg #) of each example [63] are listed in Table I. Non-analytical contributions to the dynamical matrix are also included using the formulation developed by Wang *et al.* [64]. Frequencies and other related phonon properties are calculated on a 31×31×31 mesh in the Brillouin zone: sufficient to converge the vibrational density of states and thus the corresponding thermodynamic properties. The phonon density of states is calculated using the linear interpolation tetrahedron technique available in AFLOW.

The QHA calculations are performed on 10 equally spaced volumes ranging from -3% to 6% uniform strain with 1% increments from the respective equilibrium structures of the crystal. More expanded volumes are used since most materials have positive thermal expansion. Both the SC-QHA and the QHA3P calculations are performed using ±3% expanded and compressed volumes. All calculations are performed without external pressure ($P=0$), and all volume distortions are isotropic.

RESULTS AND DISCUSSION

Thermodynamic properties of non-metallic materials from the three approaches are compared, and the same

TABLE II. RMSrD for α_V for all non-metallic materials. χ for α_V are calculated with respect to the experiments in: Ref. [39] (Si), Ref. [41] (C), Ref. [45] (SiC), Ref. [48] (ZnO), Ref. [50] (Al₂O₃), and Ref. [54] (MgO). Units: RMSrD in %.

compound	$\chi^{(\text{QHA3P, QHA})}$ % (α_V)		$\chi^{(\text{SC-QHA, QHA})}$ % (α_V)		$\chi^{(\text{QHA3P, expt})}$ % (α_V)		$\chi^{(\text{SC-QHA, expt})}$ % (α_V)	
	PBE	PBEsol	PBE	PBEsol	PBE	PBEsol	PBE	PBEsol
Si	0.1	1.3	9.2	7.5	15.7	8.4	25.8	19.6
C	0.8	1.0	2.8	4.5	14.0	12.1	16.8	12.4
SiC	0.7	0.4	4.7	3.7	13.5	12.7	12.6	11.1
ZnO	0.4	5.9	27.0	37.7	16.7	7.3	31.7	16.2
Al ₂ O ₃	0.3	0.8	11.1	9.5	12.4	8.1	18.7	9.1
MgO	0.1	1.8	27.5	14.5	25.4	14.4	75.0	38.0

TABLE III. RMSrD for α_V , C_P , and H for metallic materials and a small band gap compound. χ for α_V are computed with respect to the experiment in Refs: [20] (AlNi), Ref. [33] (NiTiSn), and Ref. [65] (Ti₂AlN). Units: RMSrD in %.

Compound	$\chi^{(\text{QHA3P, expt})}$ % ($\alpha_{V, \text{ph+elec}}$)	$\chi^{(\text{QHA3P, expt})}$ % (α_V)	$\chi^{(\text{QHA3P, expt})}$ % ($C_{P, \text{ph+elec}}$)	$\chi^{(\text{QHA3P, expt})}$ % (C_P)	$\chi^{(\text{QHA3P, expt})}$ % ($H_{\text{ph+elec}}$)	$\chi^{(\text{QHA3P, expt})}$ % (H)
AlNi	5.2	5.1	2.6	3.2	5.6	1.9
NiTiSn	6.4	6.2	0.0	0.0	n/a	n/a
Ti ₂ AlN	4.9	5.7	0.0	0.0	n/a	n/a

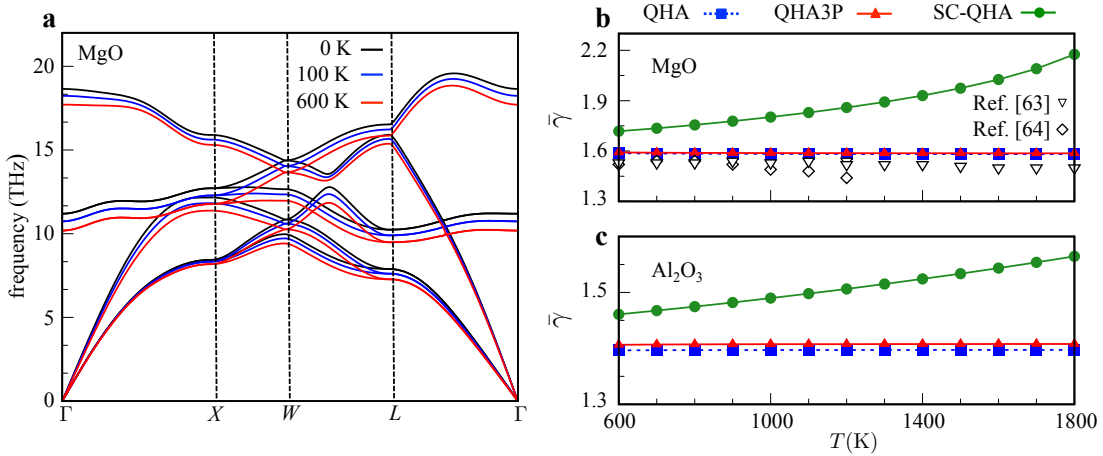


Figure 4. (a) The phonon dispersion curves of MgO at three different temperatures are computed using SC-QHA equilibrium volumes and Eq. (13). (b, c) The $\bar{\gamma}$ values as a function of temperature for MgO and Al₂O₃ using QHA3P, QHA and SC-QHA. The experimental Grüneisen parameters of MgO are taken from Ref. [54, 55].

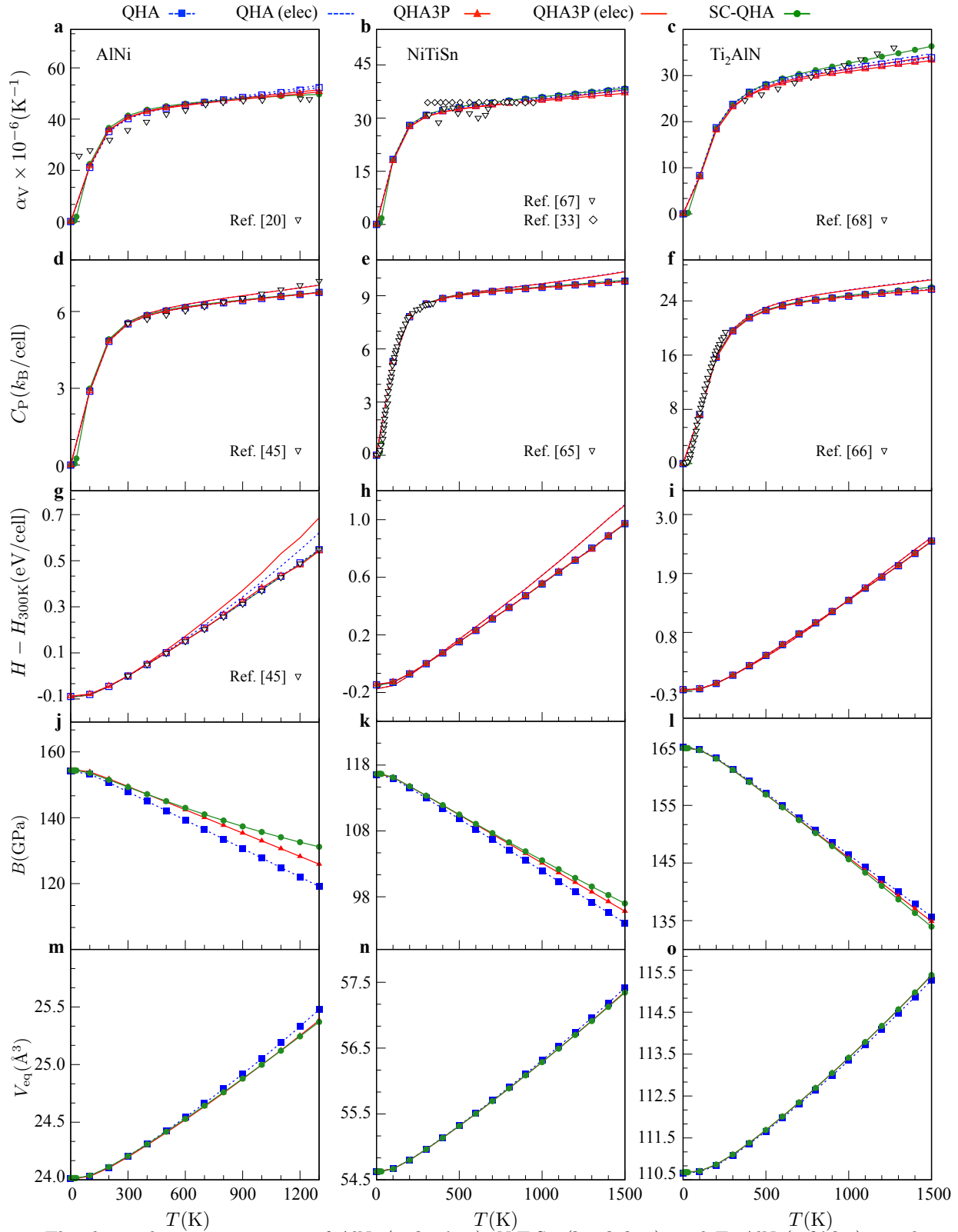


Figure 5. The thermodynamic properties of AlNi (a,d,g,j,m), NiTiSn (b,e,h,k,n), and Ti₂AlN (c,f,i,l,o) are shown up to the respective T_m of 1300 K, 1500 K and 1500 K [20, 33, 65–67], respectively. QHA3P results are compared with QHA and experiments. Experimental results from different sources [20, 33, 36, 65–67] are indicated by inverted triangles and diamonds.

methods are applied to metallic and small band gap materials.

Non-metallic compounds. The thermodynamic properties are illustrated in Figure 2 for Si, C, and SiC and in Figure 3 for ZnO, Al₂O₃, and MgO. Comparisons of QHA3P with QHA, SC-QHA, and experimental data are discussed below with two different XC functionals.

α_V from both QHA3P and QHA agree well with the available experiments for all tested non-metallic compounds using both XC functionals. Conversely, SC-QHA overestimates α_V for Si, ZnO, Al₂O₃, and MgO. Using the PBEsol XC functional improves consistency with experimental results for Si, however α_V is still larger for ZnO and MgO. For Al₂O₃, α_V values from different experiments [38, 50–52] vastly differ from one other. Below 1500 K, experimental results from Ref [50, 52] are well described by PBEsol, whereas above 1500 K, they are better predicted by PBE. The RMSrD between α_V from different approaches and experiment are provided in Table II. The relatively small RMSrD between QHA3P and experiments compared to the RMSrD between SC-QHA and experiments indicate that the QHA3P α_V predictions are more reliable.

The larger values of α_V from SC-QHA are due to the overestimation of $\bar{\gamma}$. This is particularly significant for positive α_V materials, where $\omega_j(\mathbf{q})$ decreases with T for almost all (\mathbf{q}, j) (QHA3P Methodology section). For example, the T dependent phonon dispersion curves of MgO (Figure 4(a)) show that $\omega_j(\mathbf{q})$ decreases for all (\mathbf{q}, j) , except for the acoustic branches near Γ . The $\bar{\gamma}$ values for MgO along with Al₂O₃ are illustrated in Figure 4(b, c), and are validated by experiments.

Despite differences in α_V , there are no significant differences between C_p and H obtained from the three approaches. The values are insensitive to the choice of functional, except for MgO (Figure 2 and 3(d-i)). Both C_p and H match well with the experimental values. A slight underestimation is observed for C_p for Si, SiC, and ZnO. Also, divergence from experiments occurs near 2000 K for MgO using the PBE XC functional in SC-QHA. The observations are supported by the RMSrD of C_p (Table A2, Appendix).

The values of B computed with the three methodologies also match when using the same XC functional, except for ZnO and MgO (Figure 2 and 3(j-o)). For ZnO, discrepancies are observed between the QHA3P and QHA results. Since the bulk modulus value is related to the curvature of $F(V)$ at V_{eq} , any small change in $F(V)$ leads to a larger change in B . For instance, at 2000 K the difference in F between QHA3P and QHA for ZnO is approximately 5 meV at 6% expanded volume of V_0 (Figure A1, Appendix), which significantly affects B (Figure 3(j)). The values of B calculated using PBEsol are larger than for PBE, with similar trends previously reported elsewhere [46], and are closer to experiment. For MgO, some deviation occurs at high temperature between SC-QHA and QHA3P (and QHA). RMSrD with experiment for B has not been calculated due to limited data availability. For B , the small

RMSrD values between QHA3P and QHA demonstrate that the methods are consistent with each other. The RMSrD values between SC-QHA and QHA are high for ZnO and MgO (Table A2, Appendix).

As for B , predicted V_{eq} values are similar for all of the methods when using the same XC functional. However, the volume predictions obtained using PBEsol are smaller than those for PBE (Figure 2 and 3(m-o)).

Metallic compounds and narrow band gap materials. The thermodynamic properties of the metals AlNi and Ti₂AlN and the narrow band gap (0.12 eV [68]) half-Heusler NiTiSn are presented in Figure 5. For QHA3P and QHA, calculations are performed with and without the electronic contribution. Results for SC-QHA are presented without the electronic contribution, since it is not implemented in AFLOW for this method. In this section calculations are performed only with the PBE XC functional.

Similar to the non-metallic examples, there are no prominent differences between α_V obtained using these three methods (Figure 5(a-c)). The α_V results show the effectiveness of all methodologies in accurately predicting the experimental thermodynamic properties of AlNi, NiTiSn, and Ti₂AlN. In addition, the contribution of F_{elec} to F does not alter the results.

The other thermodynamic properties, C_p , H , B , and V_{eq} , also match well with each other for these three methods and with experiments, with a few exceptions (Figure 5(d-f)). The H values for AlNi from QHA3P and QHA do not agree with experiments above 500 K when F_{elec} is taken into consideration (Figure 5(g, j)). The B values from the three methods show discrepancies stemming from the difference in the $F(V)$ energies as described in the non-metallic compounds section. The small RMSrD between QHA3P and experiment for α_V , C_p , and H indicate that the results agree well with experiments (Table III). Since the QHA, SC-QHA, and QHA3P predictions are similar, RMSrD values are presented only for QHA3P.

CONCLUSIONS

The quasi-harmonic approximation 3-phonons method is introduced to calculate thermodynamic properties of both non-metallic and metallic compounds. The efficiency of QHA3P is tested for a range of materials using two different exchange-correlation functionals, and the calculated thermodynamic quantities are in agreement with both QHA and experimental measurements. We also show that SC-QHA overestimates the average Grüneisen parameter, as well as α_V , at high temperatures for some materials, while QHA3P still performs well. This study demonstrates that QHA3P is an ideal framework for the high-throughput prediction of finite temperature materials properties, combining the accuracy of QHA with the computational efficiency of SC-QHA.

ACKNOWLEDGEMENTS

The authors acknowledge support by DOD-ONR (N00014-13-1-0635, N00014-16-1-2368, N00014-15-1-2863, N00014-17-1-2090). DH acknowledges support from the Department of Defense through the National Defense Science and Engineering Graduate (NDSEG) Fellowship Program. CO acknowledges support from the National Science Foundation Graduate Research Fellowship under Grant No. DGF1106401. SC acknowledges the Alexander von Humboldt Foundation for financial support. The consortium AFLOW.org acknowledges Duke University - Center for Material Genomics - for computational support.

APPENDIX

TABLE A1. **List of crystallographic properties.** List of compound names with various crystallographic properties along with AFLOW prototype [69, 70] and AFLOW unique identifier (auid) [5].

compound	ICSD	supercell size	supercell atoms	lattice type	sg#	DFT band gap (eV)	prototype	auid
Si	76268	5×5×5	250	fcc	227	0.61	A_cF8_227_a [71]	aflow:ff211836be789f69
C (Diamond)	28857	4×4×4	128	fcc	227	4.11	A_cF8_227_a [71]	aflow:b438e1a25f9c187d
SiC	618777	4×4×3	192	hex	186	2.30	AB_hP4_186_b_b [72]	aflow:50.644a24702c7dc
ZnO	182356	4×4×3	192	hex	186	1.81	AB_hP4_186_b_b [72]	aflow:f30df164c6192045
Al ₂ O ₃	89664	2×2×2	80	rhl	167	5.86	A2B3_hR10_167_c_e [73]	aflow:537e800e0a1b75be
MgO	159372	4×4×4	128	fcc	225	4.46	AB_cF8_225_a_b [74]	aflow:a2cc05c200330e16
AlNi	602150	4×4×4	128	cub	221	0.00	AB_cP2_221_b_a [75]	aflow:f727dcd6a292301d
NiTiSn	174568	3×3×3	81	fcc	216	0.17	ABC_cF12_216_b_c_a [76]	aflow:7bed936e9d5a44ca
Ti ₂ AlN	157766	4×4×1	128	hex	194	0.00	ABC2_hP8_194_d_a_f [77]	aflow:bdc38ae3ca07e398

TABLE A2. **List of RMSrD values.** RMSrD for C_p , and B for all non-metallic materials. χ for C_p are calculated with respect to the experiments in: Ref. [36]. χ for H and V_{eq} are similar to C_p and B , respectively, and are not presented. Units: RMSrD in %.

compound	$\chi(\text{QHA3P, expt})$ % (C_p)		$\chi(\text{SC-QHA, expt})$ % (C_p)		$\chi(\text{QHA3P, QHA})$ % (B)		$\chi(\text{SC-QHA, QHA})$ % (B)	
	PBE	PBEsol	PBE	PBEsol	PBE	PBEsol	PBE	PBEsol
Si	7.4	7.6	7.1	7.7	0.5	0.2	0.2	0.4
C	2.2	2.2	3.1	1.8	0.5	0.0	1.0	0.5
SiC	4.8	5.0	4.4	4.6	0.0	0.1	0.2	0.3
ZnO	8.5	9.3	5.9	7.0	0.3	7.0	3.4	9.8
Al ₂ O ₃	4.5	5.3	3.0	4.1	0.8	0.3	1.1	1.7
MgO	9.0	3.6	37.1	11.5	0.5	0.7	21.6	6.6

Comparison of SC-QHA from AFLOW and Ref. [30]. The SC-QHA method was originally developed and tested in Ref. [30] using the PBEsol XC functional. To check the consistency between the AFLOW implementation of SC-QHA and Ref. [30], the calculated properties are compared for Si, C, and Al₂O₃. The differences between the properties computed with AFLOW and Ref. [30] are marginal. However, some discrepancies are observed for the α_v values of Si, B values of C, and the α_v and B values of Al₂O₃, which are the presented examples in Ref. [30]. To investigate this, thermodynamic properties are reproduced for Al₂O₃ using the original SC-QHA and PHONOPY [78] codes with the AFLOW standard VASP input parameters (Figure A2, Appendix). This indicates that the origin of the incompatibility between these two studies is the difference in the VASP input parameters. While the accuracy is increased by using the AFLOW standard VASP input parameters, the results are still inconsistent with experiments and QHA.

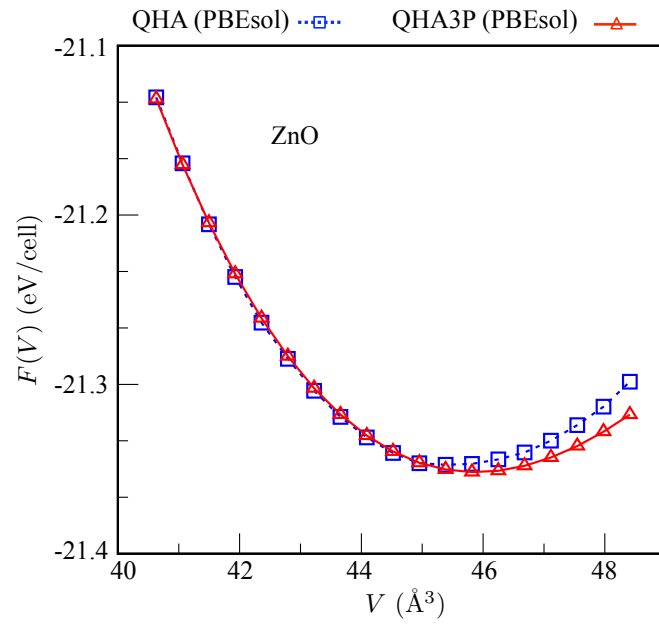


Figure A1. $F-V$ curve of ZnO. The $F(V)$ curve of ZnO at 2000 K. The range of volume is from -6 to 12 percent of V_0 (43.22 \AA^3). The difference between the two curves gives F_{vib} , since E_0 is the same for both QHA and QHA3P.

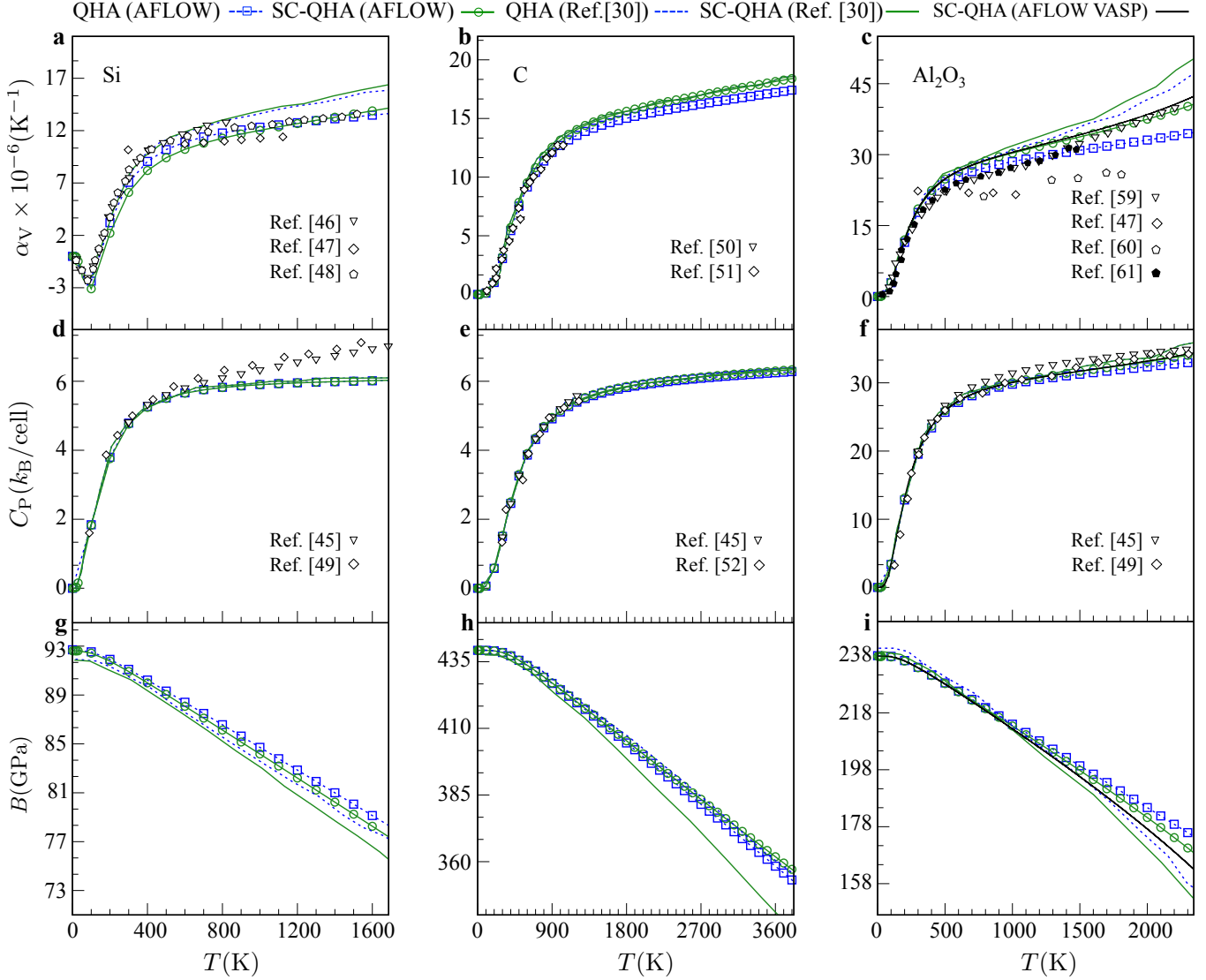


Figure A2. The comparison of AFLOW computed α_V , C_P and B with Ref. [30]. Experimental results from different sources [36–43, 45, 50–52, 54] are indicated by inverted triangles, diamonds, pentagons and filled pentagons. The black colored line for Al_2O_3 represents calculations with the PHONOPY+SC-QHA codes [30, 78], performed using the AFLOW standard VASP input parameters.

- [1] S. Curtarolo, W. Setyawan, G. L. W. Hart, M. Jahnátek, R. V. Chepulskii, R. H. Taylor, S. Wang, J. Xue, K. Yang, O. Levy, M. J. Mehl, H. T. Stokes, D. O. Demchenko, and D. Morgan, *AFLOW: An automatic framework for high-throughput materials discovery*, *Comput. Mater. Sci.* **58**, 218–226 (2012).
- [2] S. Curtarolo, W. Setyawan, S. Wang, J. Xue, K. Yang, R. H. Taylor, L. J. Nelson, G. L. W. Hart, S. Savito, M. Buongiorno Nardelli, N. Mingo, and O. Levy, *AFLOWLIB.ORG: A distributed materials properties repository from high-throughput ab initio calculations*, *Comput. Mater. Sci.* **58**, 227–235 (2012).
- [3] R. H. Taylor, F. Rose, C. Toher, O. Levy, K. Yang, M. Buongiorno Nardelli, and S. Curtarolo, *A RESTful API for exchanging materials data in the AFLOWLIB.org consortium*, *Comput. Mater. Sci.* **93**, 178–192 (2014).
- [4] A. R. Supka, T. E. Lyons, L. S. I. Liyanage, P. D’Amico, R. Al Rahal Al Orabi, S. Mahatara, P. Gopal, C. Toher, D. Ceresoli, A. Calzolari, S. Curtarolo, M. Buongiorno Nardelli, and M. Fornari, *AFLOW π : A minimalist approach to high-throughput ab initio calculations including the generation of tight-binding hamiltonians*, *Comput. Mater. Sci.* **136**, 76–84 (2017).
- [5] F. Rose, C. Toher, E. Gossett, C. Oses, M. Buongiorno Nardelli, M. Fornari, and S. Curtarolo, *AFLUX: The LUX materials search API for the AFLOW data repositories*, *Comput. Mater. Sci.* **137**, 362–370 (2017).
- [6] H. Yu, D. Duan, H. Liu, T. Yang, F. Tian, K. Bao, D. Li, Z. Zhao, B. Liu, and T. Cui, *Ab initio molecular dynamic study of solid-state transitions of ammonium nitrate*, *Sci. Rep.* **6**, 18918 (2016).
- [7] G. Kresse and J. Hafner, *Ab initio molecular dynamics for open-shell transition metals*, *Phys. Rev. B* **48**, 13115–13118 (1993).
- [8] J. Sarnthein, K. Schwarz, and P. E. Blöchl, *Ab initio molecular-dynamics study of diffusion and defects in solid Li_3N* , *Phys. Rev. B* **53**, 9084–9091 (1996).
- [9] H. L. Zhang, Y. F. Han, W. Zhou, Y. B. Dai, J. Wang, and B. D. Sun, *Atomic study on the ordered structure in Al melts induced by liquid/substrate interface with Ti solute*, *Appl. Phys. Lett.* **106**, 041606 (2015).
- [10] B. J. Jesson and P. A. Madden, *Structure and dynamics at the aluminum solid-liquid interface: An ab initio simulation*, *J. Chem. Phys.* **113**, 5935–5946 (2000).
- [11] I. Errea, M. Calandra, and F. Mauri, *First-Principles Theory of Anharmonicity and the Inverse Isotope Effect in Superconducting Palladium-Hydride Compounds*, *Phys. Rev. Lett.* **111**, 177002 (2013).
- [12] I. Errea, M. Calandra, and F. Mauri, *Anharmonic free energies and phonon dispersions from the stochastic self-consistent harmonic approximation: Application to platinum and palladium hydrides*, *Phys. Rev. B* **89**, 064302 (2014).
- [13] M. A. Blanco, E. Francisco, and V. Luaña, *GIBBS: isothermal-isobaric thermodynamics of solids from energy curves using a quasi-harmonic Debye model*, *Comput. Phys. Commun.* **158**, 57–72 (2004).
- [14] J.-P. Poirier, *Introduction to the Physics of the Earth’s Interior* (Cambridge University Press, 2000), 2nd edn.
- [15] O. Isayev, C. Oses, C. Toher, E. Gossett, S. Curtarolo, and A. Tropsha, *Universal fragment descriptors for predicting electronic properties of inorganic crystals*, *Nat. Commun.* **8**, 15679 (2017).
- [16] E. Gossett, C. Toher, C. Oses, O. Isayev, F. Legrain, F. Rose, E. Zurek, J. Carrete, N. Mingo, A. Tropsha, and S. Curtarolo, *AFLOW-ML: A RESTful API for machine-learning predictions of materials properties*, *Comput. Mater. Sci.* **152**, 134–145 (2018).
- [17] C. Toher, J. J. Plata, O. Levy, M. de Jong, M. D. Asta, M. Buongiorno Nardelli, and S. Curtarolo, *High-throughput computational screening of thermal conductivity, Debye temperature, and Grüneisen parameter using a quasiharmonic Debye model*, *Phys. Rev. B* **90**, 174107 (2014).
- [18] C. Toher, C. Oses, J. J. Plata, D. Hicks, F. Rose, O. Levy, M. de Jong, M. D. Asta, M. Fornari, M. Buongiorno Nardelli, and S. Curtarolo, *Combining the AFLOW GIBBS and Elastic Libraries to efficiently and robustly screen thermomechanical properties of solids*, *Phys. Rev. Mater.* **1**, 015401 (2017).
- [19] Z. K. Liu and Y. Wang, *Computational Thermodynamics of Materials* (Cambridge University Press, 2016), 1 edn.
- [20] Y. Wang, Z.-K. Liu, and L.-Q. Chen, *Thermodynamic properties of Al, Ni, NiAl, and Ni₃Al from first-principles calculations*, *Acta Mater.* **52**, 2665–2671 (2004).
- [21] T. Duong, S. Gibbons, R. Kinra, and R. Arróyave, *Ab-initio approach to the electronic, structural, elastic, and finite-temperature thermodynamic properties of Ti_2AX ($A = Al$ or Ga and $X = C$ or N)*, *J. Appl. Phys.* **110**, 093504 (2011).
- [22] P. Nath, J. J. Plata, D. Usanmaz, R. Al Rahal Al Orabi, M. Fornari, M. Buongiorno Nardelli, C. Toher, and S. Curtarolo, *High-throughput prediction of finite-temperature properties using the quasi-harmonic approximation*, *Comput. Mater. Sci.* **125**, 82–91 (2016).
- [23] J. M. Ziman, *Electrons and Phonons: The Theory of Transport Phenomena in Solids*, Oxford Classic Texts in the Physical Sciences (Oxford University Press, 1960).
- [24] D. C. Wallace, *Thermodynamics of crystals* (Wiley, 1972).
- [25] M. T. Dove, *Introduction to Lattice Dynamics*, Cambridge Topics in Mineral Physics and Chemistry (Cambridge University Press, 1993).
- [26] G. P. Srivastava, *The Physics of Phonons* (CRC Press, Taylor & Francis, 1990).
- [27] S. Baroni, S. de Gironcoli, A. Dal Corso, and P. Gianozzi, *Phonons and related crystal properties from density-functional perturbation theory*, *Rev. Mod. Phys.* **73**, 515–562 (2001).
- [28] A. van de Walle and G. Ceder, *The effect of lattice vibrations on substitutional alloy thermodynamics*, *Rev. Mod. Phys.* **74**, 11–45 (2002).
- [29] J. J. Plata, P. Nath, D. Usanmaz, J. Carrete, C. Toher, M. de Jong, M. D. Asta, M. Fornari, M. Buongiorno Nardelli, and S. Curtarolo, *An efficient and accurate framework for calculating lattice thermal conductivity of solids: AFLOW-AAPL Automatic Anharmonic Phonon Library*, *NPJ Comput. Mater.* **3**, 45 (2017).
- [30] L.-F. Huang, X.-Z. Lu, E. Tennesen, and J. M. Rondinelli, *An efficient ab-initio quasiharmonic approach for the thermodynamics of solids*, *Comput. Mater. Sci.* **120**, 84–93 (2016).
- [31] R. Arroyave, D. Shin, and Z.-K. Liu, *Ab initio thermo-*

- dynamic properties of stoichiometric phases in the Ni-Al system*, Acta Mater. **53**, 1809–1819 (2005).
- [32] T. Tohei, Y. Watanabe, H.-S. Lee, and Y. Ikuhara, *First principles calculation of thermal expansion coefficients of pure and Cr doped α -alumina crystals*, J. Appl. Phys. **120**, 142106 (2016).
- [33] P. Hermet, R. M. Ayrál, E. Theron, P. G. Yot, F. Salles, M. Tillard, and P. Jund, *Thermal Expansion of Ni-Ti-Sn Heusler and Half-Heusler Materials from First-Principles Calculations and Experiments*, J. Phys. Chem. C **118**, 22405–22411 (2014).
- [34] C.-L. Fu and K.-M. Ho, *First-principles calculation of the equilibrium ground-state properties of transition metals: Applications to Nb and Mo*, Phys. Rev. B **28**, 5480–5486 (1983).
- [35] J. Sólyom, *Fundamentals of the physics of solids*, vol. 1 (Springer Berlin Heidelberg, 2007), 1 edn.
- [36] I. Barin, *Thermochemical Data of pure substances* (VCH, Germany, 1993).
- [37] D. F. Gibbons, *Thermal Expansion of Some Crystals with the Diamond Structure*, Phys. Rev. **112**, 136–140 (1958).
- [38] W. M. Yim and R. J. Paff, *Thermal expansion of AlN, sapphire, and silicon*, J. Appl. Phys. **45**, 1456–1457 (1974).
- [39] Y. Okada and Y. Tokumaru, *Precise determination of lattice parameter and thermal expansion coefficient of silicon between 300 and 1500 K*, J. Appl. Phys. **56**, 314–320 (1984).
- [40] M. W. Chase Jr., *NIST-JANAF Thermochemical Tables*, Journal of Physical and Chemical Reference Data Monographs (American Inst. of Physics, 1998), fourth edition edn.
- [41] G. A. Slack and S. F. Bartram, *Thermal expansion of some diamond-like crystals*, J. Appl. Phys. **46**, 89–98 (1975).
- [42] B. J. Skinner, *The thermal expansion of theoria, periclase, and diamond*, Am. Mineral. **42**, 39–55 (1957).
- [43] A. C. Victor, *Heat Capacity of Diamond at High Temperatures*, J. Chem. Phys. **36**, 1903–1911 (1962).
- [44] H. J. McSkimin and P. Andreatch Jr., *Elastic Moduli of Diamond as a Function of Pressure and Temperature*, J. Appl. Phys. **43**, 2944–2948 (1972).
- [45] Z. Li and R. C. Bradt, *Thermal expansion of the hexagonal (4H) polytype of SiC*, J. Appl. Phys. **60**, 612–614 (1986).
- [46] G. I. Csonka, J. P. Perdew, A. Ruzsinszky, P. H. T. Philipsen, S. Lebègue, J. Paier, O. A. Vydrov, and J. G. Ángyán, *Assessing the Performance of Recent Density Functionals for Bulk Solids*, Phys. Rev. B **79**, 155107 (2009).
- [47] A. A. Khan, *X-ray determination of thermal expansion of zinc oxide*, Acta Crystallogr. Sect. A **24**, 403 (1968).
- [48] Y. S. Touloukian, R. K. Kirby, R. E. Taylor, and P. D. Desai, *Thermophysical Properties of Matter; Thermal Expansion; Nonmetallic Solids*, vol. 13 (IFI-Plenum, New York, 1977).
- [49] H. Ibach, *Thermal Expansion of Silicon and Zinc Oxide (II)*, Phys. Stat. Solidi **33**, 257–265 (1969).
- [50] S. Kondo, K. Tateishi, and N. Ishizawa, *Structural Evolution of Corundum at High Temperatures*, Jpn. J. Appl. Phys. **47**, 616 (2008).
- [51] R. G. Munro, *Evaluated Material Properties for a Sintered α -Alumina*, J. Am. Ceram. Soc. **80**, 1919–1928 (1997).
- [52] J. B. Wachtman Jr., T. G. Scuderi, and G. W. Cleek, *Linear Thermal Expansion of Aluminum Oxide and Thorium Oxide from 100° to 1100° K*, J. Am. Ceram. Soc. **45**, 319–323 (1962).
- [53] O. Madelung, U. Rössler, and M. Schulz, eds., *II-VI and I-VII Compounds; Semimagnetic Compounds* (Springer Berlin Heidelberg, Berlin, Heidelberg, 1999), doi:10.1007/b71137.
- [54] O. L. Anderson, D. Isaak, and H. Oda, *High-temperature elastic constant data on minerals relevant to geophysics*, Rev. Geophys. **30**, 57–90 (1992).
- [55] G. K. White and O. L. Anderson, *Grüneisen Parameter of Magnesium Oxide*, J. Appl. Phys. **37**, 430–432 (1966).
- [56] A. van Roekeghem, J. Carrete, and N. Mingo, *Anomalous thermal conductivity and suppression of negative thermal expansion in ScF₃*, Phys. Rev. B **94**, 020303(R) (2016).
- [57] G. Kresse and J. Hafner, *Ab initio molecular dynamics for liquid metals*, Phys. Rev. B **47**, 558–561 (1993).
- [58] C. E. Calderon, J. J. Plata, C. Toher, C. Oses, O. Levy, M. Fornari, A. Natan, M. J. Mehl, G. L. W. Hart, M. Buongiorno Nardelli, and S. Curtarolo, *The AFLOW standard for high-throughput materials science calculations*, Comput. Mater. Sci. **108 Part A**, 233–238 (2015).
- [59] P. E. Blöchl, *Projector augmented-wave method*, Phys. Rev. B **50**, 17953–17979 (1994).
- [60] J. P. Perdew, K. Burke, and M. Ernzerhof, *Generalized Gradient Approximation Made Simple*, Phys. Rev. Lett. **77**, 3865–3868 (1996).
- [61] J. P. Perdew, A. Ruzsinszky, G. I. Csonka, O. A. Vydrov, G. E. Scuseria, L. A. Constantin, X. Zhou, and K. Burke, *Restoring the Density-Gradient Expansion for Exchange in Solids and Surfaces*, Phys. Rev. Lett. **100**, 136406 (2008).
- [62] P. Nath, J. J. Plata, D. Usanmaz, C. Toher, M. Fornari, M. Buongiorno Nardelli, and S. Curtarolo, *High throughput combinatorial method for fast and robust prediction of lattice thermal conductivity*, Scr. Mater. **129**, 88–93 (2017).
- [63] D. Hicks, C. Oses, E. Gossett, G. Gomez, R. H. Taylor, C. Toher, M. J. Mehl, O. Levy, and S. Curtarolo, *AFLOW-SYM: platform for the complete, automatic and self-consistent symmetry analysis of crystals*, Acta Crystallogr. Sect. A **74**, 184–203 (2018).
- [64] Y. Wang, J. J. Wang, W. Y. Wang, Z. G. Mei, S. L. Shang, L. Q. Chen, and Z. K. Liu, *A mixed-space approach to first-principles calculations of phonon frequencies for polar materials*, J. Phys.: Condens. Matter **22**, 202201 (2010).
- [65] M. K. Drulis, H. Drulis, A. E. Hackemer, A. Ganguly, T. El-Raghy, and M. W. Barsoum, *On the low temperature heat capacities of Ti₂AlN and Ti₂Al(N_{0.5}C_{0.5})*, J. Alloys Compd. **433**, 59–62 (2007).
- [66] D. Y. Jung, K. Kurosaki, C. Kim, H. Muta, and S. Yamanaka, *Thermal expansion and melting temperature of the half-Heusler compounds: MNiSn (M=Ti, Zr, Hf)*, J. Alloys Compd. **489**, 328–331 (2010).
- [67] N. J. Lane, S. C. Vogel, and M. W. Barsoum, *Temperature-Dependent Crystal Structures of Ti₂AlN and Cr₂GeC as Determined from High Temperature Neutron Diffraction*, J. Am. Ceram. Soc. **94**, 3473–3479 (2011).
- [68] F. G. Aliev, V. V. Kozyrkov, V. V. Moshchalkov, R. V. Scolozdra, and K. Durczewski, *Narrow band in the intermetallic compounds MNiSn (M=Ti, Zr, Hf)*, Z. Phys. B: Condens. Matter **80**, 353–357 (1990).
- [69] M. J. Mehl, D. Hicks, C. Toher, O. Levy, R. M. Hanson, G. L. W. Hart, and S. Curtarolo, *The AFLOW Library of Crystallographic Prototypes: Part 1*, Comput. Mater. Sci. **136**, S1–S828 (2017).
- [70] D. Hicks, M. J. Mehl, E. Gossett, C. Toher, O. Levy, R. M.

- Hanson, G. Hart, and S. Curtarolo, *The AFLOW Library of Crystallographic Prototypes: Part 2*, arXiv:1806.07864 [cond-mat.mtrl-sci] (2018).
- [71] http://aflow.org/CrystalDatabase/A_cF8_227_a.html.
- [72] http://aflow.org/CrystalDatabase/AB_hP4_186_b_b.html.
- [73] http://aflow.org/CrystalDatabase/A2B3_hR10_167_c_e.html.
- [74] http://aflow.org/CrystalDatabase/AB_cF8_225_a_b.html.
- [75] http://aflow.org/CrystalDatabase/AB_cp2_221_b_a.html.
- [76] http://aflow.org/CrystalDatabase/ABC_cF12_216_b_c_a.html.
- [77] http://aflow.org/CrystalDatabase/ABC2_hP8_194_d_a_f.html.
- [78] A. Togo, L. Chaput, and I. Tanaka, *Distributions of phonon lifetimes in Brillouin zones*, Phys. Rev. B **91**, 094306 (2015).